

Solid-state kinetics and gas-phase prediction of 1,4-bis(trimethylsilyl)benzene

J. Selvakumar · D. Sathiyamoorthy ·
K. S. Nagaraja

Received: 15 February 2011 / Accepted: 16 June 2011 / Published online: 29 June 2011
© Akadémiai Kiadó, Budapest, Hungary 2011

Abstract The solid-state kinetics and gas-phase predictions of the 1,4-bis(trimethylsilyl)benzene (TMSB) are visualized by utilizing thermogravimetric and mass spectral data. The statistical analyses and reduced time plots of zero order (F0) and Avrami-Erofeev (A2) nucleation and growth models provides the best fit to experimental data for isothermal evaporation process for TMSB. The activation energy for non-isothermal evaporation processes of TMSB is calculated using isoconversional methods. The molecular structure and energetics of the predicted gas phase molecules and species in chemical vapor deposition process are investigated using semi-empirical quantum chemical calculations.

Keywords Organosilane · Solid-state kinetics · Isoconversional technique · Activation energy · Semi-empirical analysis

Introduction

The high melting point (~ 2973 K), satisfactory hardness (Moh's hardness of silicon carbide is 9.3/10) [1],

imperviousness to gaseous fission products, and lower reactivity to oxygen compared with pure bulk Si, of the silicon carbide (β -SiC) make it a valuable and economic coating material [2]. An important use of SiC in nuclear application is as one of the tri-isotropic (TRISO) coating layer for the uranium kernel used as the fuel in high-temperature gas-cooled nuclear reactors, which functions as a "pressure vessel" layer and is impervious to gas and metal fission products [3–5]. Experiments have provided evidence that methyltrichlorosilane is an ideal precursor for producing high quality β -SiC by chemical vapor deposition (CVD) process. However, while depositing SiC on uranium kernel at higher temperature (~ 1673 K), the byproduct of HCl will migrate toward the kernel and react with uranium forming a volatile uranium salt. The deposited SiC coatings with chlorine impurity can reduce the hardness of the coatings [6]. In the context, 1,4-bis(trimethylsilyl)benzene (TMSB) have recently received an attention because of the stability under normal condition, the volatility, free from chlorine, and ability to deposit silicon carbide films under relatively mild condition [7]. Consequently, there have been interests in the solid-state kinetics and gas-phase prediction of the TMSB for CVD applications. Thermoanalytical methods find extensive application in analysis of various materials [8, 9]. In particular thermogravimetric methods of analysis are effectively used to study the kinetics of chemical reactions [8–10]. In order to enhance the CVD process to grow high quality SiC thin films, a better understanding of the precursor gas-phase process mechanism at CVD process is desired. Hence, in this report, we described the solid-state kinetics and the gas-phase prediction of TMSB by using thermogravimetric, mass spectral fragmentation, and semi-empirical quantum chemical analyses.

J. Selvakumar (✉) · D. Sathiyamoorthy
Powder Metallurgy Division, Bhabha Atomic Research Centre,
Navi Mumbai 400 705, India
e-mail: j.maselva@gmail.com

D. Sathiyamoorthy
e-mail: dsati@barc.gov.in

K. S. Nagaraja
Department of Chemistry, Loyola Institute of Frontier Energy,
Loyola College, Chennai 600 034, India

Experimental

Thermally stimulated process—non-isothermal and isothermal

The non-isothermal TG measurements of TMSB were carried out at the heating rate ($\beta/\text{K min}^{-1}$) of 4, 6, 10, and 15 K min^{-1} with a sample size of 4–6 mg to provide a control set of values for thermal evaporation parameters. Among the several methods for the solid-state kinetics evaluation, the selected methods such as Arrhenius, Friedman, Kissinger, and Flynn–Wall were used in this article to illustrate the evaporation kinetics of TMSB from the TG weight loss data. In order to derive isothermal-evaporation kinetic parameters for TMSB, the experiments were carried out at several isothermal temperatures in the range of 373–413 K. A selected isothermal temperature was programmed and simultaneously the sample was finely powdered by using an agate mortar and pestle, spread out on a shallow platinum crucible mounted for isothermal measurements, and was carefully flushed with N_2 at a rate of $6 \text{ dm}^3 \text{ h}^{-1}$. The data generated from the above experiments were analyzed by model [11] or model-free [12] approaches to obtain Arrhenius parameters.

Gas-phase prediction—semi-empirical calculations

The pertinent information and parameters of molecular structure, total energy, heat of formation, entropy, and heat capacity for TMSB and its possible gas-phase predictions at CVD process were obtained through the calculation of the semi-empirical molecular orbital using the PM3 Hamiltonian with the help of Hyperchem 8.0.8 (evaluation copy).

Results and discussion

Non-isothermal kinetics—heating rate outcome

The effect of heating rate on the non-isothermal TG curves of the TMSB (Fig. 1) shows (i) evaporation process is in single step in the defined temperatures ranges and (ii) evaporation temperature rises with the increasing of the heating rate. The temperature variation in the weight loss rate at initial (T_i), maximum (T_p), and end (T_f) of the TMSB evaporation process are plotted against $\beta/\text{K min}^{-1}$. The resulted linear fit expressions are

$$T_i = 2.7 \pm 0.1 \beta/\text{K min}^{-1} + 351.3 \pm 1.4 \text{ K} \quad (1)$$

$$T_p = 4.3 \pm 0.2 \beta/\text{K min}^{-1} + 401 \pm 2.2 \text{ K} \quad (2)$$

$$T_f = 4.8 \pm 0.2 \beta/\text{K min}^{-1} + 417 \pm 2.2 \text{ K}. \quad (3)$$

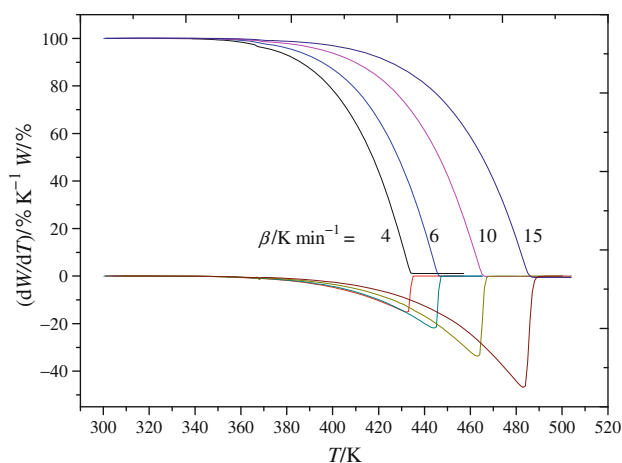


Fig. 1 The effect of the heating rate on the TG curves of the TMSB

The equilibrium evaporation temperatures are gained by extrapolating of T_i , T_p , and T_f to $\beta/\text{K min}^{-1} = 0$, and leads to 351.3 ± 1.4 , 401 ± 2.2 , and $417 \pm 2.2 \text{ K}$ for T_i^0 , T_p^0 , and T_f^0 , respectively.

Kinetic studies

In the field of thermal analysis, much attention has been directed toward the problem of obtaining kinetic information from isothermal, non-isothermal experiments. These experiments usually involve measurements of mass or heat evolved, etc., which can be related directly to the fractional reaction α , at a series of different, usually constant, heating rates ($\beta = dT/dt$) [13]. The direct estimation of activation energy is derived using Eq. 4 [14] from the various heating rate TG plots.

$$\ln \frac{d\alpha}{dT} = \ln A - \frac{E_a}{RT}. \quad (4)$$

The rate constant (k) of evaporation is given as $k = d\alpha/dT$, where $d\alpha/dT$ is the derivative of the fraction evaporated with respect to temperature. From the slope of the plots of $\ln(d\alpha/dT)$ versus $1/T$ (Fig. 2), the activation energy (E_a) for the evaporation of TMSB is calculated. The average E_a values obtained is $55.6 \pm 0.2 \text{ kJ mol}^{-1}$ for evaporation processes at different heating rates of 4, 6, 10, and 15 K min^{-1} (Fig. 1). Due to the complexity of the kinetic description concerning the solid-state evaporation processes it is usually assumed that the apparent activation energy is not a constant value but depends on α . Therefore, in order to establish if such dependence exists or not, the following kinetic procedures were adopted in this study.

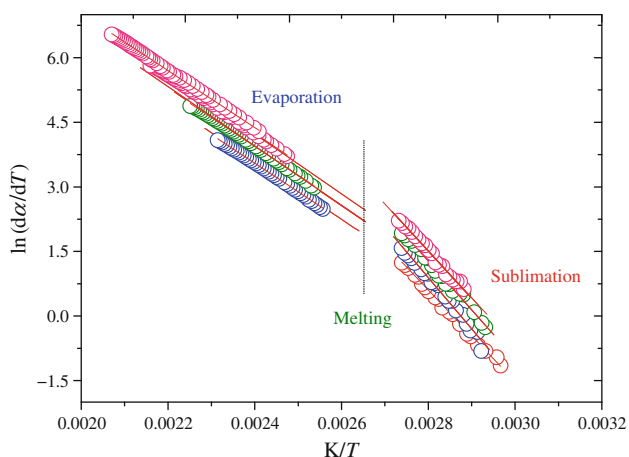


Fig. 2 Plots of $\ln(d\alpha/dT)$ against $1/T$ according to Arrhenius plots ($\beta = 4, 6, 10, \text{ and } 15$) for TMSB

Isothermal model-fitting and model-free analysis

Isothermal conditions are widely used for kinetic studies in which rates of the reaction of interest are measured at several different constant temperatures to obtain the Arrhenius parameters [15]. The calculated Arrhenius parameters from the isothermal (373, 383, 393, 403, and 413 K) plots (Fig. 3) using the model fitting method (Eqs. 5, 6) are consistent when changing the reaction model. The used model fitting expressions are

$$\ln \left[\frac{g(\alpha)}{T^2} \right] = \ln \left(\frac{AR}{\beta E_a} \right) \left(1 - \frac{2RT}{E_a} \right) - \frac{E_a}{RT} \tag{5}$$

$$\ln k(T) = \ln A - \frac{E_a}{RT} \tag{6}$$

where $g(\alpha)$ is the integral reaction model (Table 1). The reduced time plots (Fig. 4) for the isothermal evaporation of TMSB were subjected to statistical analysis as in Eqs. 7 and 8 [16]; the resulted Arrhenius parameters and F values are given in Table 2.

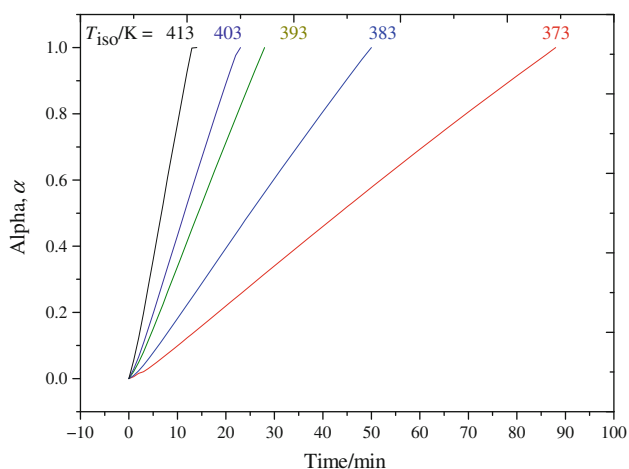


Fig. 3 Typical isothermal plots of TMSB

Table 1 Expressions for $g(\alpha)$ model functions for common mechanisms operating in solid-state reactions used in this study

Symbol	Model	Integral function $g(\alpha)$
JMA/A_n	Nucleation and growth/ $n = 1, 1.5, 2, 3, 4$	$[-\ln(1 - \alpha)]^{1/n}$
R_n	Phase-boundary controlled reaction/ $n = 1/2, 1/3$	$(1 - \alpha)^n$
F_n	Chemical process non-invoking equation/ $n = 2/3, 1/4$	$[1 - (1 - \alpha)^n]$

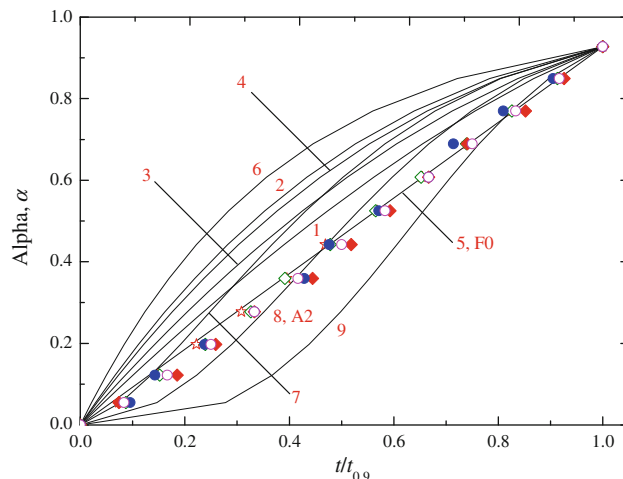


Fig. 4 Reduced time ($t/t_{0.9}$) against degree of conversion (α) plots for the evaporation of TMSB (1–9 represent the model fitting expressions). The temperature of the experiment (in Kelvin) is indicated by respective points (open circle 373 K, filled diamond 383 K, filled circle 393 K, open diamond 403 K, star 413 K)

$$S^2 = \frac{1}{n-1} \sum_{i=1}^n \left(\frac{t}{t_{0.9}} - \frac{g(\alpha)}{g(0.9)} \right)^2 \tag{7}$$

Statistics constructed as

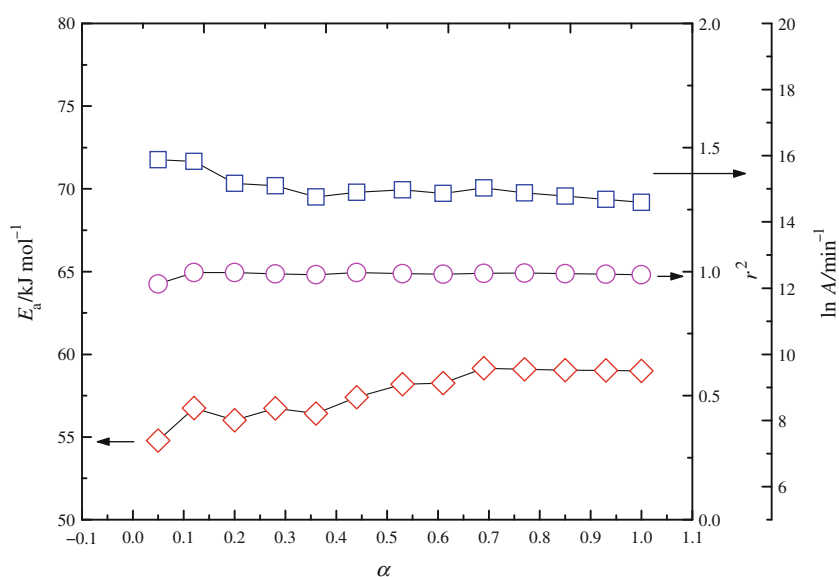
$$F = \frac{S^2}{S_{\min}^2} \tag{8}$$

The statistical analyses of reduced time plots suggest that the zero order (F0) and Avrami-Erofeev (JMA) (A2) nucleation and growth models provide the best fits to experimental data. The corresponding Arrhenius parameters are $E_a/\text{kJ mol}^{-1} = 59.7, 59.7$ and $\ln A/\text{min}^{-1} = 14.9, 15.2$ (Table 2). Therefore, the model-fitting method appears to produce quite reasonable kinetic information from isothermal data. The calculated values suggest that the thermal gasification occurs predominantly via congruent vaporization as a single-step process. These models were found to adequately describe the kinetics of evaporation of various solids, including metallorganic compounds [17, 18] and ammonium salts [19, 20].

Table 2 Arrhenius parameters for isothermal evaporation of bis(trimethylsilyl)benzene determined using the model-fitting approach (activation energy E_a , pre-exponential factor A)

No.	Model	$E_a/\text{kJ mol}^{-1}$	$\ln A/\text{min}^{-1}$	$F = S^2/S_{\min}^2$
1	F1/3 one-third order	59.7 ± 3.4	14.7 ± 1.0	547
2	F3/4 three-quarters order	59.7 ± 3.3	14.1 ± 1.0	2792
3	R2 contracting area	59.6 ± 3.4	14.5 ± 1.0	1229
4	R3 contracting volume	59.6 ± 3.4	14.3 ± 1.1	2200
5	F0 zero-order	59.7 ± 3.3	14.9 ± 1.1	1.8*
6	F1 first order	59.7 ± 3.4	15.8 ± 1.1	4948
7	A3/2 Avrami-Erofeev	59.7 ± 3.3	15.4 ± 1.0	938
8	A2 Avrami-Erofeev	59.7 ± 3.4	15.2 ± 1.1	1*
9	A3 Avrami-Erofeev	59.7 ± 3.3	14.9 ± 1.0	1532

* Best fit

Fig. 5 Arrhenius parameters against degree of conversion (α) for TMSB derived from the isothermal standard model-free (isoconversional) method (*open square* $\ln A/\text{min}^{-1}$, *open diamond* $E_a/\text{kJ mol}^{-1}$, *open circle* linear coefficient, r^2)

The isoconversional methods have their origin in the single-step kinetic equation (9) [15] and follow isoconversional principle, which states that, at a constant extent of conversion. In most of the case, the reaction rate is a function of the temperature so that the Eq. 9 rearranged and leads to Eq. 10.

$$\frac{d\alpha}{dt} = A \exp\left(\frac{-E_a}{RT}\right) f(\alpha) \quad (9)$$

$$\left[\frac{d \ln\left(\frac{d\alpha}{dt}\right)}{dT^{-1}}\right]_{\alpha} = -E_a/R. \quad (10)$$

In the above Eqs. 9 and 10, A and E_a are the Arrhenius parameters, $f(\alpha)$ is the reaction model, R is the gas constant, T is the temperature, t is the time, and α is the extent of conversion. Numerical differentiation can be avoided by using integral methods. Integration of Eq. 10 for isothermal conditions yields:

$$g(\alpha) \equiv \int_0^{\alpha} \frac{d\alpha}{f(\alpha)} = A \exp\left[\frac{-E_a}{RT}\right] t. \quad (11)$$

Rearrangement of Eq. 11 leads to Eq. 12. Application of Eq. 12 to the isothermal data for TMSB shows the functional dependence of E_a on α (Fig. 5) at different temperatures.

$$-\ln t = \ln\left[\frac{A}{g(\alpha)}\right] - \frac{E_a}{RT}. \quad (12)$$

The activation energy of the evaporation process against the extent of conversion is essentially constant, and yields a single effective value of the activation energy for the whole evaporation process is $58.3 \pm 3.4 \text{ kJ mol}^{-1}$. The derived Arrhenius parameters including linear fit residue of linear coefficient (r^2) are shown in Fig. 5.

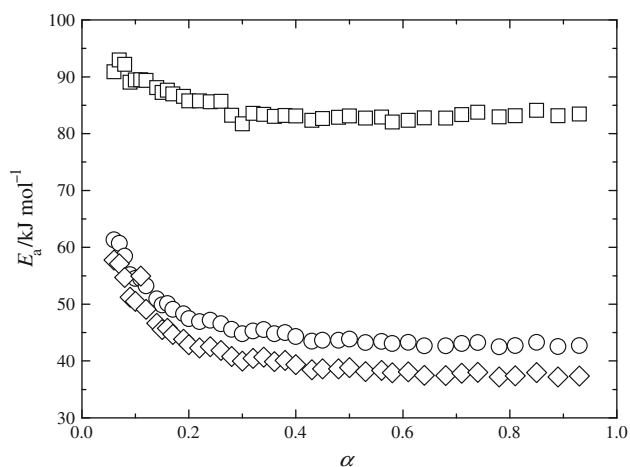


Fig. 6 Activation energy ($E_a/\text{kJ mol}^{-1}$) against degree of conversion (α) for TMSB derived from the non-isothermal model-free (isoconversional) method (open circle FWO, open diamond KAS, open square FR)

Non-isothermal isoconversional (model-free) analysis

The application of the model-free Kissinger's method (Eq. 13) [21] to the non-isothermal data for TMSB resulted in the activation energy value of $42.6 \pm 5.9 \text{ kJ mol}^{-1}$ that is slightly lower than the values obtained from isothermal processes.

$$\ln\left(\frac{\beta}{T^2}\right) \cong \ln\left(\frac{AR}{E_a}\right) - \frac{E_a}{RT} \quad (13)$$

The activation energy values derived using Eq. 14 based on Flynn–Wall–Ozawa (FWO) [22–24] is $47.1 \pm 5.2 \text{ kJ mol}^{-1}$ and Eq. 15 based on Kissinger peak methods is $43.6 \pm 1.7 \text{ kJ mol}^{-1}$ agree well with the value obtained from the Kissinger isoconversional method.

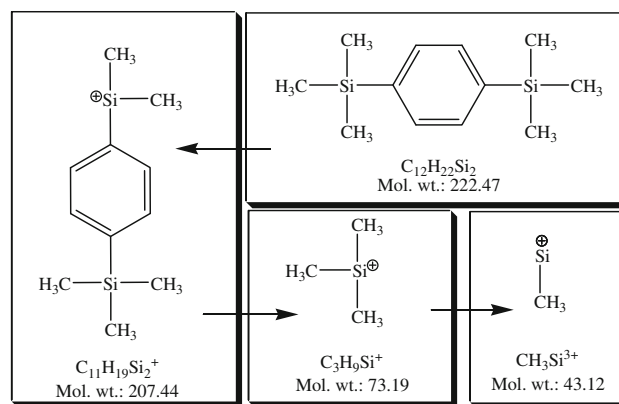
$$\ln \beta = \ln \left[\frac{AE_a}{Rg(\alpha)} \right] - 5.331 - \frac{1.052E_a}{RT} \quad (14)$$

$$\ln\left(\frac{\beta}{T^2}\right) \cong \ln\left(\frac{AR}{E_a}\right) - \frac{E_a}{RT_p} \quad (15)$$

The application of the isoconversional method for $\beta = 4, 6, 10, \text{ and } 15 \text{ K min}^{-1}$ gives an E_a dependence with a practically constant activation energy of $E_a \sim 45 \text{ kJ mol}^{-1}$ for $0.2 > \alpha < 0.9$ (Fig. 6). The E_a value from Eq. 16 suggested by the Friedman (FR) method [25] yielded a value of $85.1 \pm 3.0 \text{ kJ mol}^{-1}$.

$$\ln \left[\beta \left(\frac{d\alpha}{dT} \right) \right] = \ln(Af(\alpha)) - \frac{E_a}{RT} \quad (16)$$

where β is the heating rate, A is the pre-exponential factor, R is the gas constant, T is the absolute temperature, $g(\alpha)$ is the integral mechanism function, and α is the degree of conversion. Then, E_a was determined to be $54.6 \pm 3.9 \text{ kJ mol}^{-1}$ which was the mean value obtained by the four methods. The



Scheme 1 The possible unimolecular reaction pathway in CVD process constructed based on mass spectral data

activation energy for evaporation process is comparable with the values derived from using the isoconversional procedures.

TG and DTG—Shape method

Dollimore and co-workers [26] have proposed that the reaction model can be selected based on the shape of TG and DTG curves in non-isothermal kinetics. The reaction mechanism could be determined by considering of the following parameters: (i) the value of conversion at the maximum rate (α_m) of the reaction process (at the peak of $d\alpha/dT$ versus T curve, the peak temperature is T_m) on the $\alpha - T$ plot, (ii) the initial (T_i) and final (T_f) temperatures of the conversion curves as diffuse (d) or sharp (s), (iii) the half width (w) defined as the peak width on the curve of $d\alpha/dT$ versus T measured at half height. The half width is the parameter to distinguish different reaction mechanism in “Shape method”, which is defined as the peak width on the curve of $d\alpha/dT$ versus T measured at half height. The half width is described as

$$w = T_2 - T_1 \quad (17)$$

The half width values for each DTG curves ($\beta = 4, 6, 10, \text{ and } 15 \text{ K min}^{-1}$) were estimated using the Lorentz fit model (Eq. 18).

$$y = y_0 + (2A/\pi) \left(\frac{w}{(4^*(x - x_c)^2 + w^2)} \right) \quad (18)$$

where x_c the peak temperature, w half width, A is the area under peak, x and y are the scale parameters which specifies the w , and y_0 is the Y -value's offset. The calculated half width values are $28.3 \pm 4.2 > w > 34.9 \pm 4.1 \text{ K}$. The calculated values are compared with the “Shape method” flow chart derived by Dollimore and co-workers [26]. From the “Shape method” flow chart, the observed “ w ” values fall in the models of R2 and D2. The half width limit for R2 is $24 > w > 34$ and α_{max} limit for D2 is ≥ 0.8 to < 0.9 .

The above derived solid-state kinetic data for TMSB evaporation process discloses that (i) for isothermal evaporation, the operating mechanism for the solid-state evaporation process is F0 and A2, which means that the process solely operated by zero-order and nucleation and growth models, (ii) for non-isothermal process, the R2 (contracting area) and D2 (two dimensional diffusion) models are operating the evaporation process of TMSB, and (iii) the resulted constant activation energies from isothermal process (59.7 ± 3.3 and 58.3 ± 3.4 kJ mol^{-1}) and non-isothermal process (54.6 ± 3.9 kJ mol^{-1}) are inferred that the evaporation process is congruent (TMSB evaporating as intact) as a single-step process. The similarity of the dependencies derived from isothermal and non-isothermal measurements suggests that the operative single-step mechanism is essentially the same for the isothermal and non-isothermal conditions.

Gas-phase prediction of TMSB

The experimental or computational data on the species obtained by the gas-phase pyrolysis of TMSB is not available in the open literature. Hence, the mass spectrometric (MS) fragmentation pattern was used indirectly to suggest possible cleavage pathways during thermal decomposition of TMSB at CVD process. The caveats associated with predicting CVD behavior by MS have been discussed previously in the literature for various metallorganic compounds [27–29]. On the basis of MS information, the possible unimolecular pathway from the TMSB [$m/z = 222.47$ (15%); $\text{C}_{12}\text{H}_{22}\text{Si}_2$] is constructed in Scheme 1. In the pathway, first a methyl ($-\text{CH}_3$) group is cleaved from the TMSB molecule with concomitant formation of [$m/z = 207.44$ (100%); $\text{C}_{11}\text{H}_{19}\text{Si}_2$] $^+$. To the extent that the Scheme 1 is described the formation of [$m/$

Table 3 Molecular geometry of 1,4-bis(trimethylsilyl)benzene and its fragmentations from semi-empirical MO calculation (PM3)

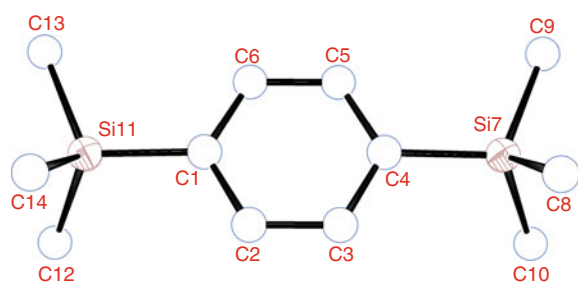
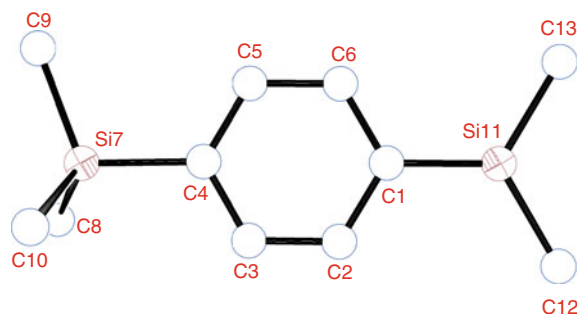
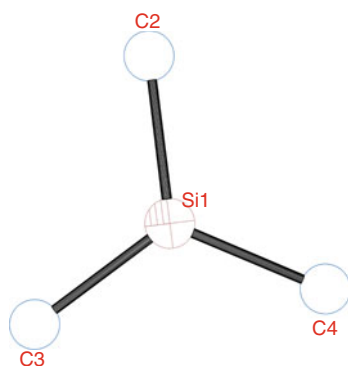
				Chemical formula = $\text{C}_{12}\text{H}_{22}\text{Si}_2$ Energies and gradient (298.15 K) Total energy = $-18431/\text{kJ mol}^{-1}$ Binding energy = $-1457.71/\text{kJ mol}^{-1}$ Heat of formation = $-28.45/\text{kJ mol}^{-1}$ Entropy = $0.6468/\text{kJ mol}^{-1}\text{K}^{-1}$ Heat capacity = $0.3135/\text{kJ mol}^{-1}\text{K}^{-1}$ Molecular point group = C_2V	
Bond distance/Å	Angles/°		Torsion angles/°		
$r(\text{C1}-\text{C2})$	1.3903	$\angle\text{C6}-\text{C1}-\text{C2}$	119.51	$\text{C6}-\text{C1}-\text{C2}-\text{H15}$	180
$r(\text{C1}-\text{C6})$	1.3886	$\angle\text{Si11}-\text{C1}-\text{C2}$	118.99	$\text{C2}-\text{C1}-\text{Si11}-\text{C14}$	59.51
$r(\text{C1}-\text{Si11})$	1.8454	$\angle\text{Si11}-\text{C1}-\text{C6}$	121.5	$\text{C6}-\text{C1}-\text{Si11}-\text{C12}$	120.49
$r(\text{C2}-\text{C3})$	1.3916	$\angle\text{C3}-\text{C2}-\text{C1}$	120.23	$\text{Si7}-\text{C4}-\text{C5}-\text{C6}$	180
$r(\text{C2}-\text{H15})$	1.0969	$\angle\text{C1}-\text{C2}-\text{H15}$	119.45	$\text{C4}-\text{Si7}-\text{C8}-\text{H19}$	176.76
$r(\text{C4}-\text{Si7})$	1.8452	$\angle\text{H15}-\text{C2}-\text{C3}$	120.32	$\text{C4}-\text{Si7}-\text{C8}-\text{H20}$	-63.17
$r(\text{C5}-\text{C6})$	1.3921	$\angle\text{C2}-\text{C3}-\text{C4}$	120.23	$\text{C4}-\text{Si7}-\text{C8}-\text{H21}$	56.77
$r(\text{C5}-\text{H17})$	1.0972	$\angle\text{C5}-\text{C4}-\text{C3}$	119.51	$\text{C9}-\text{Si7}-\text{C8}-\text{H19}$	-61.68
$r(\text{Si7}-\text{C8})$	1.8944	$\angle\text{C8}-\text{Si7}-\text{C4}$	109.09	$\text{C9}-\text{Si7}-\text{C8}-\text{H20}$	58.39
$r(\text{Si7}-\text{C9})$	1.894	$\angle\text{C9}-\text{Si7}-\text{C4}$	111.03	$\text{C9}-\text{Si7}-\text{C8}-\text{H21}$	178.33
$r(\text{C8}-\text{H19})$	1.0933	$\angle\text{C10}-\text{Si7}-\text{C4}$	109.09	$\text{C10}-\text{Si7}-\text{C8}-\text{H19}$	57.71
$r(\text{C8}-\text{H21})$	1.0938	$\angle\text{H19}-\text{C8}-\text{Si7}$	110.87	$\text{C10}-\text{Si7}-\text{C8}-\text{H20}$	177.78
$r(\text{C10}-\text{H27})$	1.0932	$\angle\text{Si7}-\text{C8}-\text{H20}$	111.08	$\text{C10}-\text{Si7}-\text{C8}-\text{H21}$	-62.28
$r(\text{Si11}-\text{C13})$	1.8939	$\angle\text{H21}-\text{C8}-\text{Si7}$	110.85	$\text{C4}-\text{Si7}-\text{C9}-\text{H24}$	60.09
$r(\text{Si11}-\text{C14})$	1.8943	$\angle\text{H20}-\text{C8}-\text{H19}$	107.98	$\text{C8}-\text{Si7}-\text{C9}-\text{H22}$	59.62
$r(\text{C12}-\text{H28})$	1.0932	$\angle\text{H21}-\text{C8}-\text{H19}$	108.04	$\text{C8}-\text{Si7}-\text{C9}-\text{H23}$	179.54
$r(\text{C13}-\text{H31})$	1.0937	$\angle\text{H22}-\text{C9}-\text{Si7}$	110.62	$\text{C8}-\text{Si7}-\text{C9}-\text{H24}$	-60.29
		$\angle\text{H23}-\text{C9}-\text{Si7}$	111.18	$\text{C10}-\text{Si7}-\text{C9}-\text{H24}$	-179.54
		$\angle\text{Si7}-\text{C10}-\text{H25}$	110.88		
		$\angle\text{C12}-\text{Si11}-\text{C13}$	109.28		

Table 3 continued



Chemical formula = $C_{11}H_{19}Si_2^+$
 Energies and gradient (298.15 K)
 Total energy = $-16763.9/kJ mol^{-1}$
 Binding energy = $-1243.27/kJ mol^{-1}$
 Heat of formation = $489.81/kJ mol^{-1}$
 Entropy = $0.5648/kJ mol^{-1} K^{-1}$
 Heat capacity = $0.2629/J mol^{-1} K^{-1}$
 Molecular point group = CS

Bond distance/Å		Angles/°		Torsion angles/°	
$r(C1-C2)$	1.4059	$\angle C2-C1-C6$	118.77	$C6-C1-C2-H14$	179.99
$r(C1-C6)$	1.4054	$\angle C2-C1-Si11$	120.66	$C3-C4-Si7-C8$	-59.46
$r(C1-Si11)$	1.7215	$\angle C6-C1-Si11$	120.56	$C5-C4-Si7-C8$	120.54
$r(C2-C3)$	1.3862	$\angle C1-C2-C3$	120.36	$C4-Si7-C8-H18$	176.52
$r(C2-H14)$	1.0985	$\angle C1-C2-H14$	119.31	$C4-Si7-C8-H19$	-63.85
$r(C4-Si7)$	1.8664	$\angle C2-C3-H15$	120.43	$C4-Si7-C8-H20$	56.89
$r(C5-C6)$	1.3862	$\angle C3-C4-C5$	119.42	$C9-Si7-C8-H18$	-63.17
$r(C5-H16)$	1.0997	$\angle C4-C5-C6$	120.53	$C9-Si7-C8-H19$	56.46
$r(Si7-C8)$	1.8869	$\angle C4-Si7-C8$	107.79	$C9-Si7-C8-H20$	177.2
$r(Si7-C9)$	1.8846	$\angle C4-Si7-C9$	110.09	$C10-Si7-C8-H18$	59.14
$r(C8-H19)$	1.0936	$\angle C4-Si7-C10$	107.79	$C10-Si7-C8-H19$	178.78
$r(C8-H20)$	1.0942	$\angle Si7-C8-H19$	111.61	$C10-Si7-C8-H20$	-60.48
$r(C10-H26)$	1.0935	$\angle Si7-C9-H21$	110.15	$C8-Si7-C9-H21$	61.08
$r(Si11-C12)$	1.8172	$\angle H22-C9-H23$	107.84	$C8-Si7-C9-H22$	-179.4
$r(Si11-C13)$	1.8175	$\angle Si7-C10-H25$	111.44	$C8-Si7-C9-H23$	-58.42
$r(C12-H27)$	1.0969	$\angle Si11-C13-H30$	113.06	$C10-Si7-C9-H21$	-61.07
$r(C13-H31)$	1.1013	$\angle H30-C13-H32$	107.26	$C10-Si7-C9-H22$	58.42
		$\angle H31-C13-H32$	106.18	$C13-Si11-C12-H28$	120.89
				$C1-Si11-C13-H30$	179.98
				$C1-Si11-C13-H31$	-59.18
				$C1-Si11-C13-H32$	59.12
				$C12-Si11-C13-H31$	120.81



Chemical formula = $C_3H_9Si^+$
 Energies and gradient (298.15 K)
 Total energy = $-5409.52/kJ mol^{-1}$
 Binding energy = $-397.18/kJ mol^{-1}$
 Heat of formation = $591.72/kJ mol^{-1}$
 Entropy = $0.3002/kJ mol^{-1} K^{-1}$
 Heat capacity = $0.0805/kJ mol^{-1} K^{-1}$
 Molecular point group = CS

Bond distance/Å		Angles/°		Torsion angles/°	
$r(Si1-C2)$	1.8008	$\angle C2-Si1-C4$	119.94	$H5-C2-Si1-C3$	180
$r(Si1-C4)$	1.7987	$\angle C3-Si1-C4$	120.31	$H6-C2-Si1-C3$	-58.83

Table 3 continued

$r(\text{C2-H5})$	1.0977	$\angle\text{Si1-C2-H5}$	114.16	C4-Si1-C2-H7	-121.16
$r(\text{C2-H6})$	1.1033	$\angle\text{H7-C2-Si1}$	111.52	H9-C3-Si1-C2	-58.92
		$\angle\text{H5-C2-H7}$	106.81	H9-C3-Si1-C4	121.08
		$\angle\text{H6-C2-H7}$	105.5	H12-C4-Si1-C2	-58.76
		$\angle\text{Si1-C3-H8}$	113.9	H12-C4-Si1-C3	121.24



Chemical formula = $\text{CH}_3\text{Si}^{3+}$
 Energies and gradient (298.15 K)
 Total energy = $-1871.27/\text{kJ mol}^{-1}$
 Binding energy = $235.83/\text{kJ mol}^{-1}$
 Heat of formation = $4180.5/\text{kJ mol}^{-1}$
 Entropy = $0.2369/\text{kJ mol}^{-1} \text{K}^{-1}$
 Heat capacity = $0.0381/\text{kJ mol}^{-1} \text{K}^{-1}$
 Molecular point group = C_3V

Bond distance/Å		Angles/°	
$r(\text{Si1-C2})$	1.6871	$\angle\text{H3-C2-Si1}$	112.91
$r(\text{C2-H3})$	1.1263	$\angle\text{H4-C2-H5}$	105.83

Table 4 Molecular geometry of 1,4-bis(trimethylsilyl)benzene from semi-empirical MO calculation (PM3) and comparison

Parameters	syn PM3 ^a	syn HF	ED	XRD
<i>Bond distances/Å</i>				
$r(\text{C1-C2})$	1.3903	1.3922	1.4086(6)	1.3994(17)
$r(\text{C2-C3})$	1.3916	1.3891	1.3974(6)	1.3946(17)
$r(\text{Si7-C4})$	1.8452	1.8967	1.8761(3)	1.8817(12)
$r(\text{Si7-C10})$	1.8944	1.8913	1.8801(3)	1.8683(17)
$\langle r(\text{C-H})_{\text{Me}} \rangle$	1.0929	1.0871	1.109	0.980
<i>Angles/°</i>				
$\angle\text{C6-C1-C2}$	119.51	116.86	117.19(18)	116.83
$\angle\text{C1-C2-C3}$	120.23	121.57	121.40(9)	121.80
$\angle\text{C1-C6-C5}$	120.26	121.58	118.7	121.80
$\angle\text{Si7-C4-C5}$	121.50	122.52	-	123.01
$\angle\text{Si11-C1-C6}$	121.50	120.62	-	120.16
<i>Torsion angles/°</i>				
C6-C1-Si11-C13	0	0	-	-67.54
C6-C1-Si11-C12	120.49	120.2	-	172.23
C3-C4-Si7-C10	59.51	59.8	-	-
C3-C4-Si7-C9	180.0	180.0	-	-
C4-Si7-C10-H31	180.0	180.0	-	-178.55
C4-Si7-C10-H32	-60.08	-60.9	-	-58.43

^a This study

$z = 73.19$ (25%); $\text{C}_3\text{H}_9\text{Si}^+$ and $[m/z = 43.12$ (17%); CH_3Si^+ ions from the $[\text{C}_{11}\text{H}_{19}\text{Si}_2]^+$ parent ion.

Molecular structure optimisations for each fragmentation were performed using PM3 Hamiltonian with the restricted Hartree-Fock (RHF) spin pairing. The optimized structure with the molecular geometry data and energy data are summarized in the Table 3. According to molecular orbital and molecular mechanics calculations, the symmetry of C_{2v} , C_s , C_s and C_{3v} are assumed for *syn*-coplaner

$\text{C}_{12}\text{H}_{22}\text{Si}_2$, $[\text{C}_{11}\text{H}_{19}\text{Si}_2]^+$, $[\text{C}_3\text{H}_9\text{Si}]^+$, and $[\text{CH}_3\text{Si}]^+$, respectively. The derived molecular geometry parameters are compared with the literature values of electron diffraction and single crystal X-ray diffraction studies (Table 4) [30, 31]. The derived molecular geometry values are comparable with the other relevant studies. The gas-phase thermochemistry and mechanisms of the reaction predictions need more experimental and theoretical investigations. In particular, the determination of bond

dissociation energies (BDE) is quite valuable, since the breaking of the weakest bond in a molecule is typically the first step in the initiation of gas-phase chemistry during CVD [32]. These semi-empirical studies and results for each possible fragmentation will be taken as a dot for DFT or ab initio studies to predict the thermochemistry and kinetics of CVD process.

Conclusions

Solid-state kinetic analyses by isothermal and non-isothermal processes revealed that the evaporation process fall on nucleation and growth and contracting area models, respectively. The isothermal process infers that Arrhenius parameter determined for the isothermal data using the model fitting method are consistent when changing the reaction model. Isoconversional method yields a single effective value of the activation energy ($58.3 \pm 3.4 \text{ kJ mol}^{-1}$) for the whole evaporation process, which is comparable with the isothermal process. Kissinger's method resulted in the average value of the activation energy (43 kJ mol^{-1}) is comparable with the activation energy values of FWO (47 kJ mol^{-1}) and Kissinger peak methods (44 kJ mol^{-1}). The formation of $[\text{CH}_3\text{Si}]^+$ cation in mass spectral fragmentation gives a confident that the possible formation of Si to C ratio (1:1) is the same as the SiC product by CVD process.

Acknowledgements The authors thank the Department of Atomic Energy (DAE)/Board of Research in Nuclear Sciences (BRNS) for financial support vide Sanction No. 2008/36/63-BRNS/4014 and for the award of Dr. K. S. Krishnan Research Associateship (KSKRA) to J. Selvakumar (No. 2010/11/1-BRNS/1079).

References

1. Lide DR. CRC handbook of chemistry and physics. 86th ed. Boca Raton: CRC Press; 2005–2006.
2. Ge Y, Gordon M, Battaglia F, Fox RO. Theoretical study of the pyrolysis of methyltrichlorosilane in the gas phase. 1. Thermodynamics. *J Phys Chem A*. 2007;111:1462–74.
3. Bukaemskiy A, Fachinger A, Bosbach D. Synthesis and properties of reaction-bonded SiC ceramic with embedded UO_2 -TRISO coated particles. *Adv Sci Technol*. 2010;73:136–41.
4. Katoh Y, Cozzi A. Ceramics in nuclear applications, vol 30. New Jersey: Wiley; 2010.
5. Dulera IV, Sinha RK. High temperature reactors. *J Nucl Mater*. 2009;383:183–8.
6. Mellor BG. Surface coatings for protection against wear. Cambridge: Woodhead Publications; 2006.
7. Selvakumar J, Sathiyamoorthy D, Nagaraja KS. Role of vapor pressure of 1,4-bis(trimethylsilyl)benzene in developing silicon carbide thin film using a plasma-assisted liquid injection chemical vapor deposition process. *Surf Coat Technol*. 2011;205:3493–8.
8. Dollimore D. Thermal analysis. *Anal Chem*. 1996;68:63R–72R.
9. Dollimore D, Lerdkanchanporn S. Thermal analysis. *Anal Chem*. 1998;70:27R–36R.
10. Vyazovkin S, Wight CA. Estimating realistic confidence intervals for the activation energy determined from thermoanalytical measurements. *Anal Chem*. 2000;72:3171–5.
11. Chrissafis K. Kinetics of thermal degradation of polymers. *J Therm Anal Calorim*. 2009;95:273–83.
12. Vyazovkin S. Model-free kinetics. *J Therm Anal Calorim*. 2007;83:45–51.
13. Galwey AK, Brown ME. Handbook of thermal analysis and calorimetry: principles and practice, vol 1. Amsterdam: Elsevier Science BV; 1998.
14. Brown ME, Dollimore D, Galwey AK. Reactions in the solid state, comprehensive chemical kinetics, vol 22. Amsterdam: Elsevier; 1980.
15. Vyazovkin S. Recent advances, techniques and applications. In: Brown ME, Gallagher PK, editors. Handbook of thermal analysis and calorimetry, vol 5. Amsterdam: Elsevier Science BV; 2008.
16. Vyazovkin S, Wight CA. Model-free and model-fitting approaches to kinetic analysis of isothermal and nonisothermal data. *Thermochim Acta*. 1999;340–341:53–68.
17. Selvakumar J, Raghunathan VS, Nagaraja KS. Sublimation kinetics of scandium β -diketonates. *J Therm Anal Calorim*. 2010;100:155–61.
18. Selvakumar J, Raghunathan VS, Nagaraja KS. Vapor pressure measurements of $\text{Sc}(\text{tmhd})_3$ and synthesis of stabilized zirconia thin films by hybrid CVD technique using $\text{Sc}(\text{tmhd})_3$, $\text{Zr}(\text{tmhd})_4$, and $\text{Al}(\text{acac})_3$ [tmhd, 2,2,6,6-tetramethyl-3,5-heptanedione; acac, 2,4-pentanedione] as precursors. *J Phys Chem C*. 2009;113:19011–20.
19. Vyazovkin S, Wight CA. Isothermal and nonisothermal reaction kinetics in solid: in search of ways toward consensus. *J Phys Chem A*. 1997;101:5653–8.
20. Vyazovkin S, Clawson JS, Wight CA. Thermal dissociation kinetics of solid and liquid ammonium nitrate. *Chem Mater*. 2001;13:960–6.
21. Kissinger HE. Reaction kinetics in differential thermal analysis. *Anal Chem*. 1957;29:1702–6.
22. Flynn JH, Wall LA. General treatment of the thermogravimetry of polymers. *J Res Natl Bur Stand A Phys Chem*. 1966;70:487–523.
23. Ozawa TA. A new method of analyzing thermogravimetric data. *Bull Chem Soc Jpn*. 1965;38:1881–6.
24. Doyle DC. Estimating thermal stability of experimental polymers by empirical thermogravimetric analysis. *Anal Chem*. 1961;33:77–9.
25. Friedman HL. Kinetics of thermal degradation of char forming plastics from thermogravimetry. applications to a phenolic plastic. *Polym Sci C*. 1963;6:183–95.
26. Gao X, Chen D, Dollimore D. The correlation between the value of α at the maximum reaction rate and the reaction mechanisms: a theoretical study. *Thermochim Acta*. 1993;223:75–82.
27. Lewkebandara TS, Sheridan PH, Heeg MJ, Rheingold AL, Winter CH. Terminal and bridging imido complexes from titanium tetrachloride and primary amines. Implications for the chemical vapor deposition of titanium nitride films. *Inorg Chem*. 1994;33:5879–89.
28. Bchir OJ, Green KM, Hlad MS, Anderson TJ, Brooks BC, Wilder CB, Powell DH, White LM. $\text{Cl}_4(\text{PhCN})\text{W}(\text{NPh})$ as a single-source MOCVD precursor for deposition of tungsten nitride (WN_x) thin films. *J Organomet Chem*. 2003;684:338–50.
29. Bchir OJ, Johnston SW, Cuadra AC, Anderson TJ, Ortiz CG, Brooks BC, Powell DH, White LM. MOCVD of tungsten nitride (WN_x) thin films from the imido complex $\text{Cl}_4(\text{CH}_3\text{CN})\text{W}(\text{N}^i\text{Pr})$. *J Cryst Growth*. 2003;249:262–74.
30. Rozsondai B, Zelei B, Hargittai I. The molecular structure of *p*-bis(trimethylsilyl)-benzene from gas phase electron diffraction. *J Mol Struct*. 1982;95:187–96.

31. Campanelli AR, Ramondo F, Domenicano A, Hargittai I. Molecular structure and conformation of *p*-bis(trimethylsilyl)benzene: a study by gas-phase electron diffraction and theoretical calculations. *Struct Chem*. 1999;10:29–40.
32. Allendorf MD, van Mol AMB. Gas-phase thermochemistry and mechanism of organometallic tin oxide CVD precursors. In: Fischer RA, editor. *Precursor chemistry of advanced materials: CVD, ALD and nanoparticles*. Berlin: Springer; 2005.